Electron-Diffraction Investigation of the Hexafluorides of Tungsten, Osmium, Iridium, Uranium, Neptunium, and Plutonium

Masao Kimura, Verner Schomaker, Darwin W. Smith, and Bernard Weinstock

Citation: The Journal of Chemical Physics **48**, 4001 (1968); doi: 10.1063/1.1669727
View online: http://dx.doi.org/10.1063/1.1669727
View Table of Contents: http://scitation.aip.org/content/aip/journal/jcp/48/9?ver=pdfcov
Published by the AIP Publishing

Electron-Diffraction Investigation of the Hexafluorides of Tungsten, Osmium, Iridium, Uranium, Neptunium, and Plutonium*

MASAO KIMURA,† VERNER SCHOMAKER,‡ AND DARWIN W. SMITH§

Gates and Crellin Laboratories of Chemistry, California Institute of Technology,|| Pasadena, California

AND

BERNARD WEINSTOCK¶

Argonne National Laboratory, Argonne, Illinois

(Received 9 August 1967)

An electron-diffraction investigation has been made by the sector–microphotometer method on WF_6, OsF_6, IrF_6, UF_6, NpF_6, and PuF_6. The photographs of all these compounds reflect a phase shift which if not accounted for leads to asymmetric structures for the molecules. It sets in at smaller values of $s=4\pi\lambda^{-1}\sin(\vartheta/2)$ the heavier the molecule and the greater the electron wavelength. There is good evidence for the symmetrical octahedral structure of all the compounds. The metal–fluorine distances were found to be 1.833 Å (W–F), 1.831 Å (Os–F), 1.830 Å(Ir–F), 1.996 Å (U–F), 1.981 Å (Np–F), and 1.971 Å (Pu–F), with estimated limits of error of ±0.008 Å except for ±0.010 Å for Pu–F.

INTRODUCTION

There are 18 hexafluoride molecules extending from sulfur to plutonium that share the common characteristic of an abnormally high volatility. For many of the heavy metals they represent the only compound of significant volatility and for most of the other elements that form hexafluorides they are the most volatile compound. There are three types of hexafluoride molecules, the Group VI nonmetal hexafluorides, xenon hexafluoride, and the transition-series hexafluorides involving $4d$, $5d$, or $5f$ nonbonding electrons. The present investigation includes three molecules in the third transition series, WF_6, OsF_6, and IrF_6, whose electronic ground-state configurations are $5d^0$, $5d^2$, and $5d^3$, and three molecules in the actinide series, UF_6, NpF_6, and PuF_6, whose electronic ground-state configurations are $5f^0$, $5f^1$, and $5f^2$. At the time that this work was undertaken it had recently been discovered that the unusual compound osmium octafluoride, OsF_8, had been incorrectly identified and the properties ascribed to it were, in fact, those of the hexafluoride, OsF_6.[1] The study of OsF_6 was then intended, in part, to serve as a corroboration of this finding. Since the experimental part of this work was completed in January 1957 seven new hexafluorides have been discovered, PtF_6,[2] RhF_6,[3] RuF_6,[4] TcF_6,[5] PoF_6,[6] XeF_6,[7] and CrF_6.[8]

The infrared and Raman spectra of hexafluoride molecules have been studied extensively, and for the vapor phase the data can be explained in terms of the structure of a regular octahedron, point group O_h, with the heavy atom at the midpoint and the six fluorine atoms at the vertices. A point of some interest would be to establish whether or not these molecules deviate to some extent from exactly regular octahedral symmetry. In particular, four of the hexafluoride molecules, ReF_6, OsF_6, TcF_6, and RuF_6, have suitable electronic degeneracy in their ground state to permit a Jahn–Teller effect.[9] Abnormalities, associated with a Jahn–Teller effect, were first noted in the vibrational spectra of the $5d$ hexafluorides ReF_6 and OsF_6,[10,11] and were confirmed when their $4d$ analogs, TcF_6[5] and RuF_6,[4] were synthesized and studied.

Most recently a comprehensive review of the vibrational properties of hexafluoride molecules provides

* This work was supported in part by the U.S. Office of Naval Research and was performed in part under the auspices of the U.S. Atomic Energy Commission. This paper is based in part on D. W. Smith's Ph.D. thesis, California Institute of Technology, 1958.

† Present address: Department of Chemistry, Faculty of Science, Hokkaido University, Sapporo, Japan.

‡ Present address; Department of Chemistry, University of Washington, Seattle, Wash.

§ Eastman Kodak Co. Predoctoral Fellow, 1957–1958. Present address: Department of Chemistry and Quantum Theory Project, University of Florida, Gainesville, Fla.

|| Contribution No. 3544.

¶ Present address: Scientific Laboratory, Ford Motor Co., Dearborn, Mich.

[1] B. Weinstock and J. G. Malm, J. Am. Chem. Soc. **80**, 4466 (1958).

[2] B. Weinstock, H. H. Claassen, and J. G. Malm, J. Am. Chem. Soc. **79**, 5832 (1957).

[3] C. L. Chernick, H. H. Claassen, and B. Weinstock, J. Am. Chem. Soc. **83**, 3165 (1961).

[4] H. H. Claassen, H. Selig, J. G. Malm, C. L. Chernick, and B. Weinstock, J. Am. Chem. Soc. **83**, 2390 (1961).

[5] H. Selig, C. L. Chernick, and J. G. Malm, J. Inorg. Nucl. Chem. **19**, 377 (1961).

[6] B. Weinstock and C. L. Chernick, J. Am. Chem. Soc. **82**, 4116 (1960).

[7] E. E. Weaver, B. Weinstock, and C. P. Knop, J. Am. Chem. Soc. **85**, 111 (1963); J. G. Malm, I. Sheft, and C. L. Chernick, *ibid.* **85**, 110 (1963); J. Slivnik, B. Brcic, B. Volavsek, J. Marsel, V. Vrscaj, A. Smalc, B. Frlec, and Z. Zemljic, Croat. Chem. Acta **34**, 187 (1962); F. B. Dudley, G. Gard, and G. H. Cady, Inorg. Chem. **2**, 228 (1963).

[8] O. Glemser, "Symposium on Inorganic Fluorine Chemistry," Argonne National Laboratory, September, 1963 (unpublished).

[9] H. A. Jahn and E. Teller, Proc. Roy. Soc. (London) **A161**, 220 (1937).

[10] B. Weinstock, H. H. Claassen, and J. G. Malm, J. Chem. Phys. **32**, 181 (1960).

[11] B. Weinstock and H. H. Claassen, J. Chem. Phys. **31**, 262 (1959).

confirmation for the assignment of O_h symmetry to all of the molecules studied, including the four Jahn–Teller molecules.[12] (A single exception is XeF_6, for which preliminary studies suggest that the structure is less symmetrical.[13]) For these four molecules the Jahn–Teller forces are "small," and a static distortion of the molecular framework does not occur, but instead the nuclear and electronic motions are coupled. A theory for this dynamic Jahn–Teller effect was first given by Moffitt *et al.*[14,15] and, independently, by Longuet-Higgins *et al.*[16] The recent reanalysis of the hexafluoride spectra substantially confirms the theory.[12]

The earliest electron-diffraction studies of hexafluoride molecules, by Pauling and Brockway[17] and by Braune and Knoke,[18] were interpreted in terms of symmetrical octahedral structures for SF_6, SeF_6, and TeF_6; Pauling and Brockway gave 1.58, 1.70, and 1.84 Å for the bond distances, and Braune and Knoke gave 1.57, 1.67, and 1.82 Å. In contrast, the electron-diffraction measurements of Braune and Pinnow[19] for the metal hexafluorides UF_6, WF_6, and MoF_6 were interpreted in terms of holohedral orthorhombic symmetry with three pairs of metal-to-fluorine distances in the proportions 1:1.12:1.22, with respective averages of 1.99 Å, 1.83 Å, and about 1.8 Å. There is also an early report[20] on OsF_6, based on its original identification as OsF_8, that the molecules of the substance are either cubes or Archimedes antiprisms, with M–F$\sim$2.5 Å.

The attempt to reconcile these unsymmetrical structures for the metal hexafluorides with the more reasonable symmetrical structure became focused on UF_6 because of the importance of this compound in its role as the process gas for the separation of the uranium isotopes by the method of gaseous diffusion. Bauer[21] repeated the electron-diffraction measurements with UF_6 vapor and concluded that the symmetrical structure was inconsistent with his data. For best agreement with his results, he derived a distorted octahedral structure with three long U–F bonds of 2.17 Å and three short ones of 1.87 Å. Such a structure was incompatible not only with the vibrational spectra but also with additional evidence that had been obtained. (A small discrepancy between the infrared and Raman data which had led the original investigators to use a Fermi resonance in their assignments of the UF_6 vibrational frequencies[22] has since been explained instead as a consequence of a large liquid–vapor shift.) The dipole moment of UF_6 was found to be negligibly small in agreement with the symmetrical structure.[23] The third-law entropy calculated from the heat capacity[24] and heat of vaporization[25] was in satisfactory agreement with the entropy calculated from the molecular data using the regular octahedral model and a symmetry number of 24 [22]; a more recent evaluation using more accurate vapor-pressure data, vibrational assignments, and equation of state[26] has confirmed and improved the agreement. Additionally, the careful x-ray determinations of Hoard and Stroupe[27] with many small cylindrical single crystals of UF_6 showed a smaller and different type of distortion of the regular octahedron in the solid than that suggested by the electron-diffraction data for the vapor. The crystals were assigned to orthorhombic holohedry, space group D_{2h}^{16}–P_{nma}, the individual molecules in the crystals having D_{4h} symmetry with four U–F distances in the plane equal to 2.02 Å and the two opposed out-of-plane distances equal to 2.13 Å. A molecular structure with a U–F distance less than 2.0 Å could be ruled out by the x-ray data.

This apparent disagreement (between the electron-diffraction data and the evidence in favor of a symmetrical structure) was resolved when Schomaker and Glauber[28] showed the fault to lie with the first Born approximation as customarily used in electron-diffraction analysis. The error, which applies generally to molecules containing both heavy and light atoms that contribute significantly to the scattering, can be removed by the use of an angle-dependent phase factor in the scattering amplitude. Glauber and Schomaker[29] derived the phase for the complex scattering factor using the second Born approximation and were able to explain the apparent split in bond length for a number of molecules containing both heavy and light atoms. Hoerni and Ibers[30] applied partial-wave scattering theory to the problem of electron scattering by U and F atoms and were able to get good agreement with observed intensity curves for UF_6 at 11 and 40 keV. Ibers and Hoerni[31] subsequently extended the

[12] B. Weinstock and G. L. Goodman, Advan. Chem. Phys. **9**, 169 (1965).
[13] L. S. Bartell, R. M. Gavin, Jr., H. B. Thompson, and C. L. Chernick, J. Chem. Phys. **43**, 2547 (1965); K. W. Hedberg, S. H. Peterson, R. R. Ryan, and B. Weinstock, *ibid.* **44**, 1726 (1966); L. S. Bartell, *ibid.* **46**, 4530 (1967).
[14] W. Moffitt and A. D. Liehr, Phys. Rev. **106**, 1195 (1957).
[15] W. Moffitt and W. Thorson, Phys. Rev. **108**, 1251 (1957).
[16] H. C. Longuet-Higgins, U. Öpik, M. H. L. Pryce, and R. A. Sack, Proc. Roy. Soc. (London) **A244**, 1 (1958).
[17] L. Pauling and L. O. Brockway, Proc. Natl. Acad. Sci. **19**, 68 (1933).
[18] H. Braune and S. Knoke, Z. Physik. Chem. (Leipzig) **B21**, 297 (1933).
[19] H. Braune and P. Pinnow, Z. Physik. Chem. (Leipzig) **B35**, 239 (1937).
[20] H. Braune and S. Knoke, Naturwiss. **21**, 349 (1933).
[21] S. H. Bauer, J. Chem. Phys. **18**, 27 (1950).
[22] J. Bigeleisen, M. G. Mayer, P. C. Stevenson, and J. Turkevich, J. Chem. Phys. **16**, 442 (1948).
[23] C. P. Smyth and N. B. Hannay, "Chemistry of Uranium (Collected Papers)." TID-5290, U.S.A.E.C.Technical Information Service Extension, Oak Ridge, Tenn. Book 2, p. 437 (1958); D. W. Magnuson, J. Chem. Phys. **24**, 344 (1956).
[24] F. G. Brickwedde, H. J. Hoge, and R. B. Scott, J. Chem. Phys. **16**, 429 (1948).
[25] B. Weinstock and R. H. Crist, J. Chem. Phys. **16**, 436 (1948).
[26] B. Weinstock, E. E. Weaver, and J. G. Malm, J. Inorg. Nucl. Chem. **11**, 104 (1959).
[27] J. L. Hoard and J. D. Stroupe, "Chemistry of Uranium (Collected Papers)." TID-5290, U.S.A.E.C. Technical Information Service Extension, Oak Ridge, Tenn., Book I, pp. 325–350 (1958).
[28] V. Schomaker and R. Glauber, Nature **170**, 290 (1952).
[29] R. Glauber and V. Schomaker, Phys. Rev. **89**, 667 (1953).
[30] J. A. Hoerni and J. A. Ibers, Phys. Rev. **91**, 1182 (1953).
[31] J. A. Ibers and J. A. Hoerni, Acta Cryst. **7**, 405 (1954).

calculation of the scattering amplitudes for 40-keV electrons from the partial-wave scattering theory to a number of other atoms for scattering angles between 0° and 28°. Wong and Schomaker, for lead tetramethyl[32] and trifluoromethyl iodide,[33] and Nazarian, for WF_6,[34] have successfully confirmed the correctness of these complex scattering amplitudes of Ibers and Hoerni. A more extensive review of the failure of the first Born approximation in the diffraction of electrons by atoms or molecules has now been given by Seip,[35] who also cites a considerable body of recent theoretical work by several authors and describes careful new experimental studies in Oslo of a series of relevant molecules including WF_6 and UF_6.

The present investigation was undertaken to enlarge the number of metal hexafluorides that had been studied by electron diffraction, and to continue the study of the phase shift by providing more extensive data at a variety of electron wavelengths for all six compounds. The initial impetus for this work was provided by a desire to characterize the molecular properties of PuF_6 [36] which at that time, similarly to UF_6, was being considered as a possible process gas for the separation of the plutonium isotopes. Owing to the extreme biological hazard presented by this study of PuF_6, a limitation on the extensiveness and completeness of these measurements was imposed. The ingestion of 2 μg of Pu in the human body is taken as a dangerous dosage.[37]

EXPERIMENTAL

The metal hexafluorides are extremely reactive and toxic compounds and are advisedly handled in a special manner for studies of their properties. The techniques used here were similar to those described in detail elsewhere.[36] The compounds studied were stored in welded nickel cylinders fitted with Monel high-pressure valves. They were manipulated in an all-metal manifold constructed of nickel and Monel pipe and assembled with Monel high-pressure fittings and valves. A three-stage metal oil diffusion pump provided the necessary high-vacuum, ultimate pressure of 10^{-7} mm Hg. Uranium hexafluoride and iridium hexafluoride were prepared similarly to osmium hexafluoride[1] in a simple fluorine-gas-flow system; the preparations of neptunium hexafluoride[38] and plutonium hexafluoride[36] are described elsewhere; the sample of tungsten hexafluoride was taken from a commercially available source.[39] All of the samples were purified by distillation techniques whose effectiveness have been demonstrated in other applications having similar requirements, such as infrared spectroscopy.[36]

The samples were introduced into the diffraction apparatus through a stainless-steel tube with a final nozzle section 1 mm long and 0.3 mm in inside diameter. The rate of flow through the nozzle was regulated by adjusting the vapor pressure of the sample behind it with a cooling bath. For the compounds studied, the range of temperature control was between −23° and −55°C.

The diffraction pictures were made with a rotating-sector, Kodak process plates, a camera distance of about 9.6 cm, and various electron wavelengths as indicated in Table I. The actual wavelength values used have an estimated standard deviation of about 0.1%, on the basis of the consistency of the ZnO measurements (at 34, 40, and 47 keV) made to calibrate the voltage divider.

The interest in studying the radioactive gases NpF_6 and PuF_6 made it desirable to give special attention to the possibility of the spread of the radioactivity and to anticipate the need for decontamination of the diffraction chamber. An externally manipulated valve designed especially to minimize the spread of the admitted gases throughout the diffraction equipment was installed inside the diffraction chamber. The valve body consisted of a closed cylindrical copper tube coaxial with the nozzle and provided with a series of interior cylindrical fins. The valve was cooled with liquid nitrogen and acted as a condenser for all the effusing gas that struck it. To close the valve, the copper tube was seated against a confined Teflon ring. When the valve was closed, the copper cylinder could be evacuated through the hexafluoride manifold described previously. With the valve open, the only aperture provided was for the incident electron beam above, and diffracted cones of electrons below. The efficacy of this arrangement was tested with CCl_4: A small amount of the gas was admitted through the nozzle while the valve was cooled and open with the electron beam on; subsequently, the valve was closed and warmed to room temperature, and the CCl_4 was distilled back into the gas-handling manifold. A quantitative measurement was impossible in the system used, but within the limits of accuracy of the Bourdon gauge provided, a substantial recovery had been effected.

In practice, however, the valve was simply closed at the end of the experiment and removed for eventual separate decontamination, no attempt being made to recover the radioactive fluoride gases in the way just described: the small amounts used in the diffraction studies were rendered effectively involatile by reaction

[32] C. H. Wong and V. Schomaker, J. Chem. Phys. **28**, 1007 (1958).
[33] C. H. Wong and V. Schomaker, J. Chem. Phys. **28**, 1010 (1958).
[34] G. Nazarian, Ph.D. thesis, California Institute of Technology, (1957).
[35] H. M. Seip, in *Selected Topics in Structure Chemistry* (Universitetsforlaget, Oslo, 1967), pp. 26–68.
[36] B. Weinstock and J. G. Malm, J. Inorg. Nucl. Chem. **2**, 380 (1956); A. E. Florin, I. R. Tannenbaum, and J. F. Lemons, *ibid.* **2**, 368 (1956); C. J. Mandleberg, H. K. Rae, R. Hurst, G. Long, D. Davies, and K. E. Francis, *ibid.* **2**, 358 (1956).
[37] Natl. Bur. Std. (U.S.), Handbook 69, 87 (1959).
[38] J. G. Malm, B. Weinstock, and E. E. Weaver, J. Phys. Chem. **62**, 1506 (1958).
[39] General Chemical Division, Allied Chemical and Dye Corp., 40 Rector St., New York, N.Y.

TABLE I. MF_6 photographs: Temperatures, acceleration potentials, and wavelengths.[a]

M	t	$V=47$ $\lambda=0.055$	40 0.060	34 0.066	24 0.079	12 0.112	11 0.114	6 keV 0.160 Å
W	−55°C	×	×	×	×	×		×
Os	−39°		×			×		
Ir	−42°		×				×	
U	−25°	×	×				×	
Np	−23°	×	×				×	
Pu	−27°	×	×				×	

[a] The ×'s denote the acceleration potentials used for each compound.

on the valve surfaces, as were the small fractions that entered the camera through the beam aperture and contaminated the interior walls of the diffraction chamber and the photographic plates. Radioactivity amounting in order of magnitude to about 1% of the total activity used became fixed in the emulsion and did not wash off in the subsequent treatment of the plates. This provided a potential hazard during the measurements with the plates, but no actual difficulties from this source were experienced. Decontamination of the diffraction chamber was effected without incident by swabbing with toluene and xylene; dilute aqueous $Al(NO_3)_3$–HNO_3 solution was comparatively ineffective, presumably because of a film of organic material provided by the pump oil. A demountable cold trap downstream showed no activity, so that the hexafluorides apparently have a high sticking probability; indeed, very little activity was found anywhere in the camera except in regions close to the cone defined by the gas jet and the exit opening of the valve.

ANALYSIS OF THE DIFFRACTION DATA

Theory

Electron scattering by gas molecules containing both heavy and light atoms was discussed by Schomaker and Glauber[28,29] and by Hoerni and Ibers,[30,31] and more recently by others including Seip.[35] For electrons of wavelength λ scattered at angle ϑ, the scattering factors f_j for atoms are *complex* functions $[f_j=|f_j|\exp(i\eta_j)]$ of λ, ϑ, and the atomic number Z_j, rather than the *real* functions obtained by using the first Born approximation. The expression for the total scattered intensity is

$$I_t(s)=B(s)+K\sum_{ij}{}'\,|f_i(s)\,||f_j(s)\,|\cos\Delta\eta_{ij}(s)\times\exp(-\sigma_{ij}^2s^2/2)\,(\sin r_{ij}s)\,r_{ij}^{-1}s^{-1} \quad (1)$$

with $s=4\pi\lambda^{-1}\sin(\vartheta/2)$; B is the background or structure-independent scattering; K is a constant scale factor; the prime indicates that terms with $i=j$ are to be omitted; $\Delta\eta_{ij}$ is the difference $\eta_i-\eta_j$ between the phase angles of the scattering factors f_i and f_j; and σ_{ij} is the root-mean-square variation of r_{ij}, the distance between atoms i and j, due to vibration. The second term (the molecular part) in the right member of Eq. (1) may be called I_m so that we have $I_t=B+I_m$.

For precise sector work, especially where a determination of the σ_{ij} is desired, theoretical intensity curves $I_c(s)$ may be computed from the expression

$$I_c(s)=s[I_t(s)-B(s)]/K\,|f_k(s)\,||f_l(s)\,|=\sum_{ij}{}'\,C_{ij}(s)r_{ij}^{-1}\cos\Delta\eta_{ij}(s)\,\exp(-\sigma_{ij}^2s^2/2)\,\sin r_{ij}s \quad (2)$$

with

$$C_{ij}(s)=|f_i(s)\,||f_j(s)\,||f_k(s)\,|^{-1}\,|f_l(s)\,|^{-1} \quad (3)$$

and compared with experimental curves $I_e(s)$ defined by

$$I_e(s)=s[I_t(s)_{\rm obs}-B'(s)]/K\,|f_k(s)\,||f_l(s)\,|. \quad (4)$$

Here, f_k and f_l are scattering factors for a particular important pair of atoms in the molecule (or may be some sort of average scattering factors), and are introduced for convenience instead of the full theoretical or experimental background, the purpose in either case being to give the pattern the familiar appearance of a sum of damped sine waves. Further, $I_t(s)_{\rm obs}$ is the total observed electron intensity, allowance being made for the presence of the sector, and $B'(s)$ may be either an experimental or a theoretical background curve.

For regular octahedral MF_6 molecules, Eq. (2) may be written as

$$I_c(s)=6r^{-1}\cos\Delta\eta\,\sin rs\,\exp[-\tfrac{1}{2}(\sigma_{\rm MF}^2s^2)]+12C_{\rm FF}2^{-1/2}r^{-1}\sin\sqrt{2}rs\,\exp[-\tfrac{1}{2}(\sigma_{\rm F\cdot F}^2s^2)]+3C_{\rm FF}2^{-1}r^{-1}\sin 2rs\,\exp[-\tfrac{1}{2}(\sigma_{\rm F\cdot\cdot F}^2s^2)], \quad (5)$$

with $r=r_{\rm MF}$, $\Delta\eta=\Delta\eta_{\rm MF}$, and $C_{\rm FF}=|f_{\rm F}(s)\,||f_{\rm M}(s)\,|^{-1}$ [using $k=$M, $l=$F in Eq. (3)]. (The "shrinkage" and anharmonicity effects are small for these molecules[40,35] and were neglected.) The reason that the early electron-diffraction studies of UF_6 were misinterpreted is that $\Delta\eta$ increases monotonically with s, and can be roughly approximated as $\Delta\eta=s\delta$ with δ constant.[29] With this approximation, the factor $6r^{-1}\cos\Delta\eta\sin rs$ in Eq. (5) becomes

$$3r^{-1}[\sin(r+\delta)s+\sin(r-\delta)s]=3[(r+\delta)^{-1}\sin(r+\delta)s+(r-\delta)^{-1}\sin(r-\delta)s]+O(\delta/r^2). \quad (6)$$

[40] E. Meisingseth, J. Brunvoll, and S. J. Cyvin, Kgl. Norske Videnskab. Selskabs Skrifter **1964**, No. 7.

Because Eq. (6) corresponds to the sum of terms contributed by a split pair of distances $r_{ij}=r_0+\delta$ and $r_{ij}'=r_0-\delta$, UF_6 was interpreted as having three short and three long U–F bonds. This is easily seen in the diffraction pattern: the amplitude of the MF term reaches zero and changes sign at a point ($s=s_c$), determined by $\Delta\eta=\pi/2$, called the cutoff point. However, the electron-diffraction pattern for UF_6 and the other hexafluorides in this and previous studies[30,34] can be adequately explained, if proper scattering theory is used, on the basis of a regular octahedral model with all U–F bond distances equal, as will be shown in the succeeding sections of this paper.

Intensity Curves and Least-Squares Adjustment

Microphotometer traces of the plates were made with an instrument incorporating an RCA 1P 39 phototube and, to damp out part of the noise due to photographic imperfections, a resistance–capacitance electronic filter circuit. The signal was amplified by an Applied Physics Corporation vibrating-reed electrometer, and recorded with a Brown recording potentiometer.

By use of a rotating stage fitted to the microphotometer it was possible to spin the photographic plates about their centers, and so average out graininess and defects in the emulsion and reduce the effect of any possibly unsymmetrical spurious background caused by apparatus scattering.

In order to correct for the nonlinearity of the photographic emulsion[41] one needs two plates at different exposures of the same exact diffraction pattern, developed together. However, in the present work, the electron accelerating voltage was changed with every exposure in a set of consecutive plates because of limited amounts of some of the samples and because of the primary purpose of determining the effect of the voltage on the diffraction pattern. Therefore, no correction was or could be made for the nonlinearity of the photographic emulsion, and the experimental intensity curves were obtained on the assumption that the photographic density was proportional to the electron intensity: they are in error by being multiplied by a smooth function of s. However, this will not affect the determinations of bond distances and relative vibrational amplitudes, nor will it alter the characteristic features of the reduced diffraction pattern. It *will* preclude the determination of reliable absolute vibrational amplitudes.

Experimental intensity curves I_e were obtained by replacing the denominator of Eq. (4) by an empirical background B'':

$$I_e=s(I_{t,\text{obs}}-B')/B'',$$

where $I_{t,\text{obs}}$ was assumed proportional to the photographic density, corrected for the presence of the sector, B' was an empirical background curve, drawn by hand through the diffraction rings, and B'' was a version of

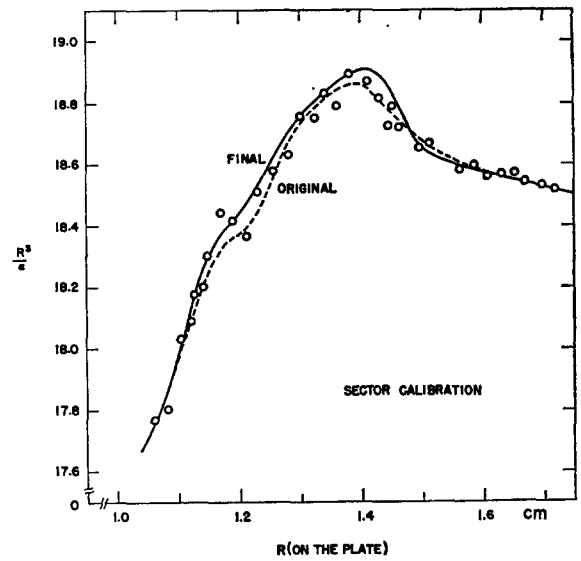

FIG. 1. Original (– – –) and final (——) sector calibration curves near 1.4 cm. The radius R corresponds to distances on the photographic plate, and α is the angular sector opening in radians.

B' adjusted where necessary to conform to the general shape of the expected theoretical background. This adjustment was necessary because of the nonideal character of the background, caused perhaps by spurious apparatus scattering and by trouble with the sector calibration as discussed below. Dividing by an empirical or semiempirical background curve rather than the theoretical expression in Eq. (4) partially compensates for the nonlinearity of the photographic emulsion.

The sector was designed to have an angular opening α proportional to R^3 for values of the radius R greater than 1.27 cm. For R less than 1.27 cm, the opening was made greater in order to give a flat background with carbon compounds (for which the sector was originally designed). The sector deviates markedly from its intended shape at 1.1–1.2 cm and at 1.3–1.5 cm.[42] Further, the sector calibration curve (a plot of R^3/α), which was obtained by use of a traveling microscope, is not very accurate at small R, where α is so small that large errors are introduced into R^3/α.

In the process of refining models, the region of the sector calibration curve corresponding to about 1.4 cm on the plate (one of the regions of difficulty just mentioned) had to be redrawn a number of times. A calibration curve was finally selected that would fit the calibration points fairly well and yet lead to experimental intensity curves having reasonable agreement with theoretical curves. This calibration curve for the region of difficulty is shown in Fig. 1, along with the measured calibration points and the curve originally drawn.

The structural parameters were obtained by fitting theoretical intensity curves I_c to the experimental

[41] J. Karle and I. L. Karle, J. Chem. Phys. **18**, 957 (1950).

[42] Wong and Schomaker also discussed discrepancies which arose in visual work with this sector (see Ref. 33).

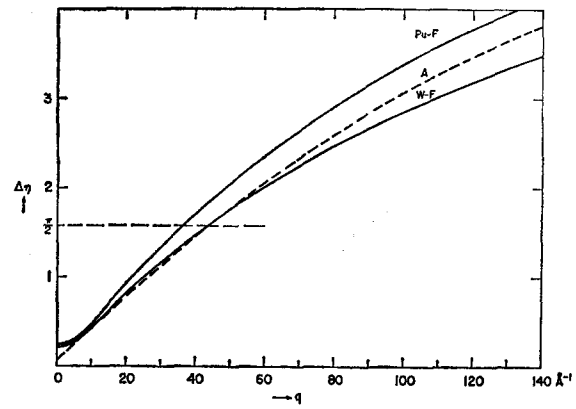

FIG. 2. Dependence of phase shift $[\Delta\eta(\vartheta)]$ on scattering angle $[q=40\lambda^{-1}\sin(\vartheta/2)]$ for 40-keV electrons: Pu-F and W-F (——) from calculations by Ibers and Hoerni (Ref. 31), A (– – –) $\Delta\eta_{W\text{-}F}$ approximated by Eq. (8).

curves by the method of least squares. The preliminary calculated intensity curves were based on radial distribution curves obtained by Fourier inversion of each set of diffraction data, approximating the integral[43]

$$rD(r)=\int I_e \sin rs\,ds \qquad (7)$$

by a summation[44] using integral values of $q=10s/\pi$. The radial distribution curves all have two major peaks of about equal weight and separated by a few tenths of an angstrom, the separation depending on the wavelength. Arising from the metal–fluorine bond distance, these peaks are split in consequence of the difference in phase angle discussed in the previous section.

Theoretical curves $I_c(s)$ were obtained[44] using Eq. (5) with the following approximations. First, it was considered adequate to approximate $C_{FF}=|f_F(s)||f_M(s)|^{-1}$ in Eq. (5) by a constant independent of s. Actually, C_{FF} is a slowly decreasing function of s, but this approximation will be partially compensated for by the use of slightly larger vibrational amplitudes $\sigma_{F.F}$ and $\sigma_{F..F}$ than would otherwise be needed. Second, $\Delta\eta$ was approximated for computational convenience by the expression

$$\Delta\eta=(\pi/2)+2\pi[a(q-q_c)+b(q-q_c)^2], \qquad q=10s/\pi, \qquad (8)$$

which gives a curve of the same general shape as the theoretical $\Delta\eta$ of Hoerni and Ibers[30] and involves three adjustable parameters: the cutoff point q_c, where the amplitude of the MF term reaches zero; a, which fixes the gradient $(\partial\Delta\eta/\partial q)_{q=q_c}=2\pi a$ at the cutoff point; and b, which similarly fixes the curvature. The data proved insufficient to determine all three parameters precisely, whereupon b was given the same fixed value, -0.0000129, throughout. This arbitrary choice of b roughly matches the theoretical curvature; to the extent that it is in error, it has of course induced error in our other results, especially q_c, a, and the σ^2's. Unfortunately, this point was not explored.

In Fig. 2, $\Delta\eta$ as approximated by Eq. (8) is shown as a broken line, with a and q_c taken from the final least-squares refinement of WF_6 at 40 keV. The fit to the theoretical curve shown for WF_6 is better than 10% over the whole range of interest, with very good agreement at q_c in magnitude but not in slope.

The coefficients C_{ij} in Eq. (2) were determined from an average theoretical value of the ratio

$$|f_i||f_j||f_M|^{-1}|f_F|^{-1}$$

using the $|f|$'s of Ibers and Hoerni.[31]

The effect of varying the C_{ij} was studied during the least-squares refinement of the 40-keV WF_6 data. The first row of Table II corresponds to the A_i obtained from the scattering amplitudes of Ibers and Hoerni[31] for $q=50$ and the second row to those for $q=65$; as expected, the corresponding changes in a and the σ's were small—less than the standard deviations. The atomic-number approximation $f\propto Z$ (last row) caused larger differences, but in no case was r (1.830 Å throughout) or q_c appreciably affected. The amplitude ratios used in the final least-squares refinements were 1000:285:50 for WF_6, OsF_6, and IrF_6; and 1000:278:50 for UF_6, NpF_6, and PuF_6.

The following parameters in the calculated curves I_c were adjusted by least squares: the metal–fluorine distance r_{MF}; the cutoff point q_c; the three vibrational amplitudes σ_{MF}, $\sigma_{F.F}$, and $\sigma_{F..F}$; the phase-shift parameter a; and an arbitrary scale factor K. Essentially, the procedure of Bastiansen, Hedberg, and Hedberg[45] was followed, minimizing the sum of weighted squares of residuals $\sum_q p(q)[V(q)]^2$, where $p(q)$ is a weighting function, and $V(q)=I_e(q)-I_c(q)$ is the difference between the experimental and theoretical intensity curves. The weighting function was $p(q)=(q-1)\times\exp(-1.2\times10^{-5}\pi^2q^2)$, whereas Bastiansen *et al.*,[45] used the closely similar function $p=s\exp(-0.0012s^2)$.

The least-squares program used the analytical expressions for the partial derivatives of I_c with respect

TABLE II. WF_6 at 40 keV. Effect of varying the amplitude factors $A_{ij}=C_{ij}/r_{ij}$. Subscripts: 1↔WF; 2↔F·F; 3↔F··F; dimensions: σ and a (Å); q_c (Å^{-1}). $A_1=1000$.

A_2	A_3	σ_1	σ_2	σ_3	q_c	a
300	55	0.0379	0.0944	0.0654	43.9	0.00503
285	50	0.0386	0.0936	0.0650	43.9	0.00496
174	30	0.0395	0.0665	0.0356	43.7	0.00414

[43] J. Waser and V. Schomaker, Rev. Mod. Phys. **25**, 671 (1953).

[44] The calculation of the radial distribution functions, as well as the calculation of the theoretical intensity functions and the least-squares refinement, were performed on the Burroughs 205 digital computer. Programs written by one of us (D.W.S.) are available through the Burroughs Company.

[45] O. Bastiansen, L. Hedberg, and K. Hedberg, J. Chem. Phys. **27**, 1311 (1957).

to all parameters except r_{MF}, where the derivative was approximated by differences based on increments of 0.005 Å in r_{MF}. The adjustment procedure is an iterative process, and the computer was programmed to adjust the parameters automatically and perform successive iteration cycles at the discretion of the machine operator.

After several least-squares cycles, it was apparent that the original background was in error, so a smooth correction line was drawn by eye, using difference curves I_e-I_c as a guide. This adjustment to the background followed the general trend of I_e-I_c over regions of 30 to 50 q units or so, but not the shorter-range

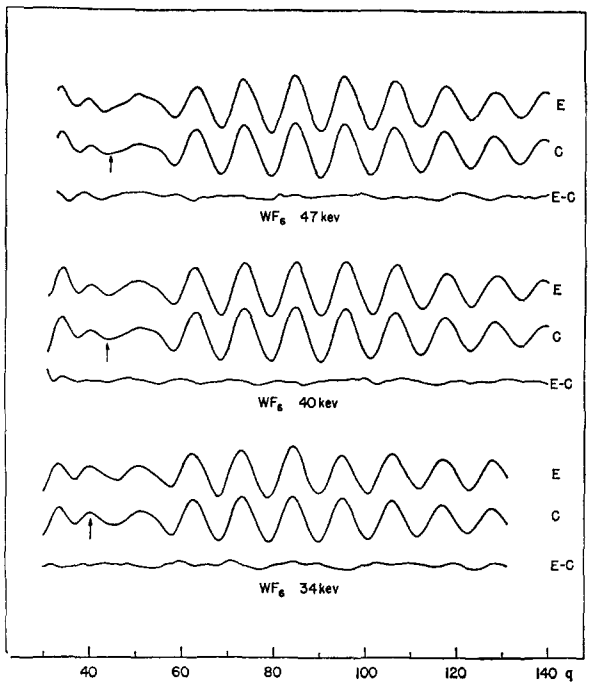

FIG. 3. Experimental (E), calculated [by Eqs. (5) and (8), see text] (C), and difference (E−C) intensity curves for WF_6 at 47, 40, and 34 keV. The arrow indicates the position of the cutoff point on each calculated curve.

fluctuations. Least-squares refinement was then continued through several more cycles, until no further change in the parameters occurred.

RESULTS AND DISCUSSION

Tables III–VIII give the final structural and phase-shift parameters as obtained by least squares; the corresponding theoretical and experimental intensity curves are compared in Figs. 3–8. For PuF_6, as discussed below, the least-squares adjustment was done only on the 11-keV data.

Table IX summarizes the structural results as averaged over the data at different electron wavelengths for each compound; it also includes Seip's results for WF_6 and UF_6. The external estimates of standard deviation reported in Tables III–VIII are based on the

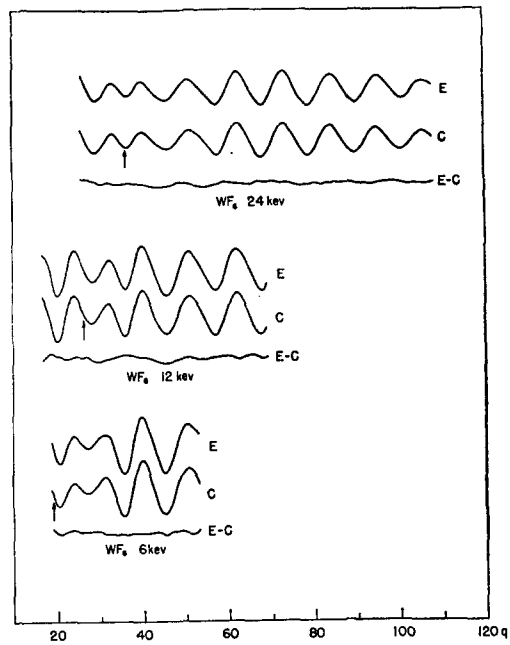

FIG. 4. Experimental (E), calculated [by Eqs. (5) and (8), see text] (C), and difference (E−C) intensity curves for WF_6 at 24, 12, and 6 keV. The arrow indicates the position of the cutoff point on each calculated curve.

assumption that the observations (at $\Delta q=1$) are independent. The estimates are therefore probably too small, the observations being differences between intensity values read from a smoothed curve drawn through the experimental points and values read from

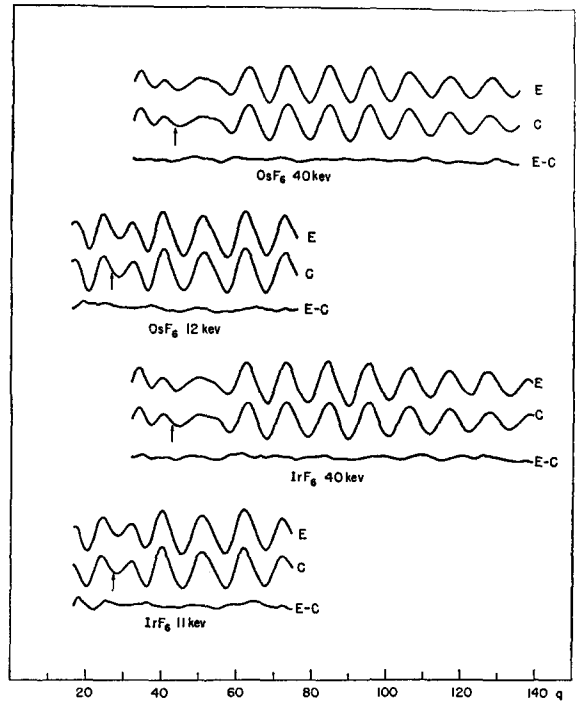

FIG. 5. Experimental (E), calculated [by Eqs. (5) and (8), see text] (C), and difference (E−C) intensity curves for OsF_6 and IrF_6. The arrow indicates the position of the cutoff point on each calculated curve.

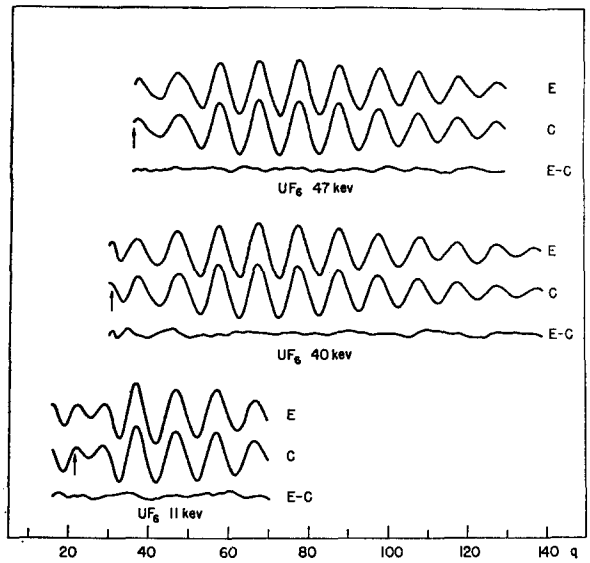

FIG. 6. Experimental (E), calculated [by Eqs. (5) and (8), see text] (C), and difference (E−C) intensity curves for UF_6. The arrow indicates the position of the cutoff point on each calculated curve.

the final smooth but still uncertain background curve, and so being subject to correlated errors rather than randomly independent errors. Such correlation of errors implies the use of a nondiagonal weight matrix[46] in the least-squares analysis, but we shall simply apply a rough rule that Hedberg has used,[45] namely that the apparent standard deviation should be multiplied by a factor of about $\sqrt{2}$ in order to compensate for correlation, although Murata[47] suggests that in the present cases the effect may not be so great. The uncertainty in distance scale due to uncertainties in the electron wavelengths and the camera distance is estimated to be 0.2%. Based on these considerations, the limit of error (twice the standard deviation) would be about 0.008 to 0.014 Å in the bond lengths, depending on the particular set of data; limits of error for the final, average values are reported in Table IX.

The limits of error on the relative mean-square vibrational amplitudes $\sigma_2^2-\sigma_1^2$ and $\sigma_3^2-\sigma_1^2$ (Table IX) are difficult to fix, and probably should be somewhat higher than the values given, which are the average deviations from the mean for the $(\sigma_i^2-\sigma_j^2)$ values

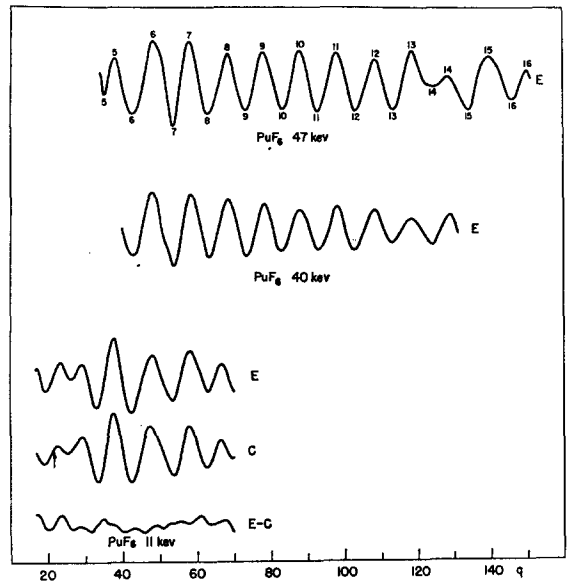

FIG. 8. Experimental (E), calculated [by Eqs. (5) and (8), see text] (C), and difference (E−C) intensity curves for PuF_6. The arrow indicates the position of the cutoff point on each calculated curve.

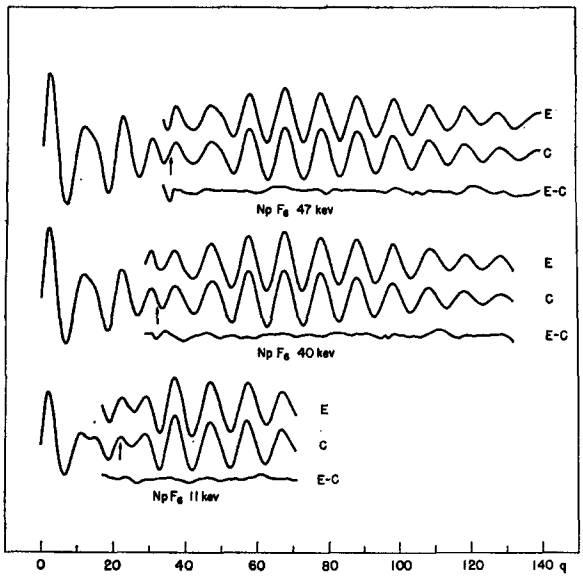

FIG. 7. Experimental (E), calculated [by Eqs. (5) and (8), see text] (C), and difference (E−C) intensity curves for NpF_6. The arrow indicates the position of the cutoff point on each calculated curve.

obtained at the various electron wavelengths. Moreover, diffusion of the scattering gas along the electron beam increases the effective value of σ^2, and the more so the greater the interatomic distance, which may just possibly be responsible for the seeming tendency of the $\Delta\sigma^2$'s obtained to be somewhat larger than the ones calculated by Kimura and Kimura,[48] also shown in Table IX, and by Meisingseth *et al.*,[40] neither of which are based on spectroscopic assignments that are still acceptable in all respects.[12] The agreement is fairly good, nevertheless, being poorest for WF_6, for which, however, Seip[35] reports that Weinstock and Goodman's assignment[12] leads to good agreement for σ_2 (and $\sigma_2^2-\sigma_1^2$), if not for σ_3. In any case, there is much

[46] Y. Morino, K. Kuchitsu, and Y. Murata, Acta Cryst. **18**, 549 (1965).

[47] Y. Murata (private communication).

[48] M. Kimura and K. Kimura, J. Mol. Spectry. **11**, 368 (1963).

TABLE III. Least-squares refinement for WF_6.[a]

	47 keV	40 keV	34 keV	24 keV	12 keV	6 keV
$10^4 r$	18 360(7)	18 290(6)	18 360(7)	18 280(9)	18 280(16)	18 380(19)
$10 q_c$	443(6)	439(4)	403(6)	365(5)	270(6)	193(7)
$10^3 \sigma_1$	35(4)	39(3)	40(4)	51(4)	70(4)	52(9)
$10^3 \sigma_2$	90(8)	94(6)	100(9)	106(10)	129(7)	109(9)
$10^3 \sigma_3$	43(12)	65(14)	67(18)	56(14)	90(16)	85(17)
$10^4 a$	50(4)	50(4)	46(5)	52(6)	31(7)	31(6)

[a] Tables III–VIII list the best values (and standard deviations) for the metal–fluorine distance r, the cutoff point q_c, the MF, F·F, and F··F vibration amplitudes σ_1, σ_2, and σ_3, and the slope parameter a of Eq. (8). The standard deviations are external estimates of random errors and are probably too small by about the factor $2^{-1/2}$ (see text). The σ's are especially subject to systematic errors, so that only the differences of σ^2's quoted in Table IX have much prospect of physical significance. Units: r and σ (Å); q_c (Å^{-1}).

better agreement with Seip's distances and amplitudes than could have been expected in view of the estimated errors. Our estimates of error for the bond lengths seem to be too large by a factor of 2 or more, and the remarkable constancy in the series WF_6 to IrF_6 and the contrasting decrease in the series UF_6 to PuF_6 are much better established than we have dared to claim from our work alone.

The experimental and theoretical cutoff points q_c are compared in Table X, where the indicated limits of error are $8^{1/2}$ times the standard deviations listed in Tables III–VIII ($\sqrt{2}$ to compensate for correlated observations and 2 to convert from standard deviation to limit of error). The 0.2% systematic scale error is negligible in this connection. The theoretical q_c's were either interpolated graphically from the η values given for Thomas–Fermi atoms by Ibers and Hoerni[31] or, for energies other than the 40-keV value for which their calculations were made, were obtained by use of their approximation formula.[31] For the 6–12 keV range, however, Ibers and Hoerni's table does not extend high enough in atomic number to calculate q_c by the approximation formula. The value for UF_6 at 11 keV is from the earlier paper by Hoerni and Ibers,[30] and like the value given there for UF_6 at 40 keV, it is based on a Hartree wavefunction for fluorine and the Thomas–Fermi model for uranium. The theoretical and experimental cutoff points show rough agreement in the way q_c decreases with the electron wavelength and with the atomic number Z: The change in q_c with Z is small within each of the groups W, Os, and Ir and U, Np, and Pu but quite large between the two groups, as was already known, and is large over the range of wavelengths explored, which in range of wavelength and number of examples is the still unique feature of this aspect of our study. The agreement with the theoretical values of q_c is better for the longer than for the shorter wavelengths, and is poor at the shortest wavelengths. It is possible that some of this disagreement is due to error in the theoretical values, which in view of Seip's tests at 35 keV[35] cannot be expected to be as accurate as the ones that could now be obtained. More of the discrepancy is probably to be attributed to error in the experimental values, however, because it is just for these short-wavelength points, indicated by parentheses in Table X, that the experimental q_c might be especially subject to error, in view of our use of only one, doubtlessly too-large, beam stop. It would be unreasonable to expect q_c to be well determined when it falls near or at the lower limit of observation, whereupon the least-squares determination could only become excessively sensitive to our assumption of an arbitrarily fixed value of the curvature b in Eq. (8). More experiment is needed.

The PuF_6 pictures are poor, but because of the toxicity hazard no further attempt was made to obtain good ones. Least-squares refinement was impossible for the 47- and 40-keV data. Although visible rings extend to large angles of scattering, the amplitudes of the maxima and minima on the photometer traces are small compared to those of the other compounds, and it was impossible to get good photometer traces.

TABLE IV. Least-squares refinement for OsF_6.

	40 keV	12 keV
$10^4 r$	18 320(5)	18 300(13)
$10 q_c$	432(4)	268(6)
$10^3 \sigma_1$	44(2)	63(3)
$10^3 \sigma_2$	87(6)	112(8)
$10^3 \sigma_3$	70(13)	73(18)
$10^4 a$	45(4)	42(5)

TABLE V. Least-squares refinement for IrF_6.

	40 keV	11 keV
$10^4 r$	18 320(6)	18 290(14)
$10 q_c$	428(4)	267(5)
$10^3 \sigma_1$	44(2)	64(5)
$10^3 \sigma_2$	93(7)	93(9)
$10^3 \sigma_3$	80(17)	42(24)
$10^4 a$	43(4)	74(7)

TABLE VI. Least-squares refinement for UF_6.

	47 keV	40 keV	11 keV
$10^4\,r$	19 990(5)	19 950(7)	19 940(16)
$10\,q_c$	359(8)	306(9)	220(6)
$10^3\,\sigma_1$	49(6)	49(6)	71(9)
$10^3\,\sigma_2$	126(11)	133(13)	118(13)
$10^3\,\sigma_3$	73(15)	73(18)	74(26)
$10^4\,a$	48(8)	48(7)	78(8)

In particular, the amplitudes of max 6 and min 7 of the 47-keV curve are excessive and the shape of the 14th ring is implausible. From the results on UF_6 and NpF_6 at 47 keV, the 47-keV PuF_6 cutoff should be in the range $q=30$–36. In comparison with the calculated curves for UF_6 at 40 keV ($q_c=30.6$) and UF_6 at 47 keV ($q_c=36.1$) in Fig. 6, the nearly symmetrical shape of min 6 and the relatively large excursion from max 6 to min 7 (possibly in error) of the experimental 47-keV PuF_6 curve then favor the lower value of q_c, whereas the shoulder on max 6 favors the higher; increasing q_c beyond 36 would quickly bring profound disagreement. The relative amplitudes of the fourth, fifth, and sixth rings would immediately fix q_c more precisely (see Fig. 7 where the theoretical curves for NpF_6 extend to smaller scattering angles), but the fourth ring was hidden by the beam stop.

Because there are no data below $q=40$ for PuF_6 at 40 keV, about all that can be said is that q_c is less than 40. The unexpected shelf at $q=52$ ($R=1.54$ cm) is not due to the troublesome 1.4-cm region of the sector. Max 6 and min 7 have excessive amplitudes in this case also.

The Pu–F distance was found by comparing the positions of maxima and minima of the 47- and 40-keV experimental curves with those of the corresponding calculated curves for NpF_6. These results are given in Tables XI and XII.

The results of the least-squares refinement for PuF_6 at 11 keV are shown in Fig. 8 and Table VIII. The best theoretical curve agrees with the experimental curve in the aspects that can be judged visually, such as the height of max n relative to the average of the heights of maxima $(n+1)$ and $(n-1)$, but the difference curve leaves much to be desired. The results are generally less certain than for the other compounds, and the σ's are especially unreliable—the least-squares adjustment even made $\sigma_{F..F}^2$ negative. Therefore, $\sigma_{F..F}$ was set to zero and its least-squares adjustment suppressed.

TABLE VII. Least-squares refinement for NpF_6.

	47 keV	40 keV	11 keV
$10^4\,r$	19 830(8)	19 820(6)	19 770(15)
$10\,q_c$	359(11)	328(6)	222(6)
$10^3\,\sigma_1$	54(5)	53(5)	69(8)
$10^3\,\sigma_2$	117(15)	128(10)	109(12)
$10^3\,\sigma_3$	77(20)	90(20)	77(27)
$10^4\,a$	42(10)	51(6)	78(9)

TABLE VIII. Least-squares refinement for PuF_6 at 11 keV.

$10^4\,r$	19 580(26)
$10\,q_c$	216(10)
$10^3\,\sigma_1$	31(20)
$10^3\,\sigma_2$	43(15)
$10^3\,\sigma_3$	...
$10^4\,a$	111(4)

The present investigation of UF_6 extends the work of Hoerni and Ibers,[30] who found fairly satisfactory agreement with the visual curves obtained from 40- and 11-keV photographs by using complex scattering amplitudes and a symmetrical octahedral model with $r_{UF}=2.00$ Å, $\sigma_{F\cdot F}^2-\sigma_{UF}^2=44\times10^{-4}$ Å^2, and $\sigma_{F..F}^2-\sigma_{UF}^2=15\times10^{-4}$ Å^2. Our results seem to agree well with these earlier ones at 11 keV, but our calculated curve for 40 keV is in better agreement with both our sector data and the visual curve by Bastiansen which Hoerni and Ibers tried to fit. Nevertheless, our 40-keV UF_6 cutoff is probably too small, perhaps because of the too-large beam stop and the assumption on b, and the

TABLE IX. Grand-average structural results.[a]

		$10^4\,(\sigma_2^2-\sigma_1^2)$[b]		$10^4\,(\sigma_3^2-\sigma_1^2)$[b]	
	$10^3 r_{M-F}$	Obs	Calc[c]	Obs	Calc[c]
WF_6	1833(8)[e]	74(10)[d]	57	24(12)[d]	12
WF_6[f]	1832±3	88±12		36±17	
OsF_6	1831(8)	70(16)	63	22(8)	13
IrF_6	1830(8)	58(12)	66	22(22)	14
UF_6	1996(8)	126(24)	119	22(12)	17
UF_6[f]	1999±3	129±25		18±26	
NpF_6	1981(8)	104(24)	104	32(14)	17
PuF_6	1971(10)	...	99	...	19

[a] All distances in angstroms.
[b] Subscripts for $\sigma_i^2-\sigma_j^2$: $i=1, 2, 3 \leftrightarrow$ M–F, F·F, F··F.
[c] Estimated limit of error; see text.
[d] Average deviation; see text.
[e] From spectroscopic data by Kimura and Kimura, Ref. 48.
[f] Electron-diffraction final results by Seip, Ref. 35, the r_{M-F} values, unlike ours, being corrected for anharmonicity. The standard deviations (±3 for $10^3 r_{M-F}$, etc.) include "an estimate of systematic errors." For the standard deviations of the $\sigma_i^2-\sigma_j^2$, the errors of the σ_i were assumed to be independent.

TABLE X. Experimental and theoretical cutoff points q_c.

	Z_M	keV	Experimental		Theoretical		Δq_c[a]
WF_6	74	47	44.3(1.7)[b]		49.5		5.2
		40	43.9(1.1)	42.9[c]	43.7		−0.2
		35		40.0[d]			
		34	40.3(1.7)		40.9		0.6
		24	36.5(1.4)		37.0		0.5
		12	27.0(1.7)		...		
		6	[19.3(2.0)][f]		...		
OsF_6	76	40	43.2(1.1)		42.7		−0.5
		12	26.8(1.7)		...		
IrF_6	77	40	42.8(1.7)		42.2		−0.6
		11	27.6(1.4)		...		
UF_6	92	47	[35.9(2.3)]		41.9		6.0
		40	[30.6(2.5)]	34.0[e]	37.0	34.6[e]	6.4
		35		31.8[d]			
		11	22.0(1.7)		23.0		1.0
NpF_6	93	47	[35.9(3.1)]		41.5		5.6
		40	[32.8(1.7)]		36.8		4.0
		11	22.2(1.7)		...		
PuF_6	94	47	...		41.1		
		40	...		36.5		
		11	21.6(2.8)		...		

[a] Ibers and Hoerni (Ref. 31, see text) vs the present experiments.
[b] Limits of error; see text.
[c] Nazarian (Ref. 34).
[d] Seip (Ref. 35).
[e] Hoerni and Ibers (Ref. 30).
[f] Values rendered unreliable by lack of sufficient data at or below q_c; see text.

Glauber and Schomaker and Hoerni and Ibers values are probably better, agreeing more closely with Seip's experimental results and theoretical calculations—but all indicate that the Ibers and Hoerni theoretical q_c for UF_6 at 40 keV is too high.

Our results on WF_6 at 40 keV are also in satisfactory agreement with those of Nazarian,[34] who found $r_{WF}=1.834$ Å, $\sigma_{F\cdot F}^2-\sigma_{WF}^2=44\times10^{-4}$ Å^2, $\sigma_{F..F}^2-\sigma_{WF}^2=16\times10^{-4}$ Å^2, and $q_c=42.9$ Å^{-1} by the correlation method with visual data. (Note that the visual-correlation method, in agreement with the general experience with it, gave good results here for WF_6 and UF_6 for both r_{MF} and q_c but not for the σ's, especially $\sigma_2^2-\sigma_1^2$.) The experimental and theoretical cutoff points agree, but Fig. 2 shows that the slopes of $\Delta\eta$ vs q at q_c do not, and it is to be emphasized that the expression (8) adjusted by least squares was flexible enough to have allowed the slopes to match if the data had demanded it. In this respect, we have not attempted a detailed comparison of our 40-keV WF_6 results with Seip's, which are no doubt more accurate.

In conclusion, our data provide strong further evidence that the apparent splits of bond distances are

TABLE XI. Electron-diffraction data for PuF_6 at 47 keV.[a]

	Minima		Maxima	
No.	q_{obs}	q/q_{obs}	q_{obs}	q/q_{obs}
5	35.18	(0.971)	37.83	0.994
6	42.76	0.995	48.20	0.986
7	53.84	0.998	53.18	0.999
8	63.44	0.998	68.64	0.992
9	73.77	0.996	78.21	1.001
10	83.72	0.997	88.15	1.002
11	93.13	1.004	98.05	1.005
12	103.62	1.000	108.56	1.001
13	113.75	1.000	118.44	1.004
14	124.02	0.999	128.64	1.000
15	134.54	0.995	139.38	0.997
16	145.83	0.987	150.14	0.992

[a] Average, 23 features, 0.997$_4$; average deviation, 0.004; $r_{Pu-F}=1.983$ Å × 0.997 = 1.977 Å.

TABLE XII. Electron-diffraction data for PuF_6 at 40 keV.[a]

	Minima		Maxima	
No.	q_{obs}	q/q_{obs}	q_{obs}	q/q_{obs}
5			39.06	(0.960)
6	42.54	1.007	47.69	1.003
7	54.06	0.986	58.57	0.990
8	63.63	0.992	68.68	0.989
9	73.67	0.992	78.37	0.996
10	83.01	1.003	88.04	1.002
11	93.17	1.000	98.01	1.002
12	102.61	1.007	108.47	0.999
13	113.44	0.999	118.29	1.009
14	124.38	0.993	128.96	0.996

[a] Average, 18 features, 0.998$_0$; average deviation, 0.006; $r_{Pu-F}=1.982$ Å × 0.998 = 1.978 Å.

not real, for if the characteristic inversion in the pattern were due to this cause, the cutoff point q_c would not show the observed changes with electron wavelength. Although there is only rather rough agreement between the experimentally derived and the theoretical phase shifts $\Delta\eta$ and cutoff points q_c—and this deficiency is considerably reduced in Seip's newer studies, both by better experimentation and by the use of better theoretical f's (atomic scattering amplitudes)—there can be no doubt about the fact that deviations from octahedral symmetry are no longer required when appropriate complex scattering amplitudes are used. Small distortions from octahedral symmetry cannot be ruled out on the basis of the diffraction data, to be sure, but nothing of the magnitude typically reported in the electron-diffraction literature before 1952.

THE JOURNAL OF CHEMICAL PHYSICS VOLUME 48, NUMBER 9 1 MAY 1968

Convexity of the H Function: The Weak-Coupled Master Equation

S. HARRIS

College of Engineering, State University of New York at Stony Brook, Stony Brook, New York

(Received 18 December 1967)

We show, for the weak-coupled master equation, that the choice of H function which preserves the usual relationship with the thermodynamic entropy is convex as a function of time.

INTRODUCTION

In a recent paper McKean has conjectured, solely on the basis of mathematical considerations, that the particular property of Boltzmann's H function which singles it out from the class of functionals of the Boltzmann equation solution may be that its successive derivatives alternate in sign.[1] In order for this conjecture to be meaningful one must first show that the derivatives of the H function possess this alternating property. For a simple model of a gas we have shown that the H function does have this property.[2] We have also shown that for a hard sphere gas a particular physical significance can be attached to the requirement that Boltzmann's H function be a convex function of the time, i.e., that $d^2H/dt^2 \geq 0$.[3] The proof of this statement however appears to be a difficult proposition, and for the Boltzmann equation, this is still an open question. In the present paper, we show that when the kinetic description is given by the weak-coupling master equation (the Pauli equation) the appropriate H function is convex. This result represents the first demonstration of the convexity property for a rigorously derived kinetic equation.

The weak-coupled master equation can be written in the following form[4]:

$$dP_i/dt = \sum_j (A_{ji}P_j - A_{ij}P_i). \tag{1}$$

Here P_i, the master function, is the probability of a state i, and A_{ij} is the transition probability per unit time from states i to j. Equation (1) can be shown to be rigorous in the weak-coupled approximation in the so-called $\lambda^2 t$ limit (see below).[5] In this approximation the A_{ij} are stationary and are of order λ^2, where λ is the coupling constant. Further, the A_{ij} satisfy the following detailed balance equation:

$$A_{ij}P_i^0 = A_{ji}P_j^0, \tag{2}$$

where P_i^0 is the value of P_i in equilibrium. The detailed balance equation $A_{ij}=A_{ji}$ is sometimes used; from (2) we see that this result is only valid for particular ensembles (e.g., a uniform ensemble, a microcannonical ensemble, but not, e.g., a cannonical ensemble). In order to stay as general as possible we will use the detailed balance equation given by (2).

In what follows we must pay particular attention to the approximations inherent in (1), as it is rigorously derived, with respect to the ordering of the various terms in the coupling constant. We have already noted that the A_{ij} are of order λ^2. The left-hand side of (1) is also of order λ^2; this follows from the fact that the perturbation expansion in λ through which (1) is derived is only meaningful in the so-called $\lambda^2 t$ limit, $\lambda \to 0$, $t \to \infty$, $\lambda^2 t =$ finite.[5] Finally, terms of order λ^3 and higher are neglected on the right-hand side of (1). We can formally explicate the degree of approximation implicit in (1) by writing

$$P_i = P_i^0[1+\lambda p_i + O(\lambda^2)], \tag{3}$$

and considering, instead of (1), the following equation:

$$dp_i/dt = \sum_j A_{ij}(p_j - p_i). \tag{4}$$

[1] H. McKean, Jr., Arch. Rational Mech. Anal. **21**, 343 (1966).
[2] S. Harris, J. Math. Phys. **8**, 2407 (1967).
[3] S. Harris, J. Chem. Phys. **48**, 3600 (1968).
[4] S. A. Rice and P. Grey, *The Statistical Mechanics of Simple Liquids* (Interscience Publishers, Inc., New York, 1965), Chap. 3.
[5] G. V. Chester, Rept. Progr. Phys. **26**, 411 (1963).